Hybrid Glide-Symmetric Unit Cell for Leakage Reduction in Millimeter-Wave PCB Interconnections to Waveguide Components

David González-Gallardo, Astrid Algaba-Brazález, Lars Manholm, Martin Johansson, *Senior Member, IEEE*, and Oscar Quevedo-Teruel, *Senior Member, IEEE*

***Abstract*— In this article, we propose a hybrid glide-symmetric metasurface which presents an electromagnetic bandgap (EBG) behavior at the *Ka*-band. The innovative part of this work is the hybrid nature of the periodic structure, which is implemented with holes on two different technologies: printed circuit board (PCB) and metallic waveguide. These holes avoid propagation in an undesired parallel plate created between a PCB and a metallic waveguide. To demonstrate the potential of this concept, a hybrid glide-symmetric configuration was placed surrounding a PCB–waveguide transition at the *Ka*-band to reduce the leakage created by undesired air gaps. A prototype was manufactured and measured to corroborate the effectiveness of this technique to reduce losses and crosstalk.**

***Index Terms*— 5G, 6G, glide symmetry, leakage suppression, millimeter-waves, printed circuit board (PCB), periodic structures, substrate-integrated hole (SIH), waveguide.**

I. Introduction

COMMUNICATIONS users are demanding more traffic capacity, shorter latency, and less energy consumption. These demands are aimed to be satisfied with the new generations of communications, known as 5G and 6G. To fulfill these expectations, 5G and beyond need more bandwidth which can only be obtained allocating new frequency bands [1]–[3]. The low-frequency spectrum (sub-6 GHz) is exceedingly crowded, and hence *Ka* and millimeter bands have been chosen for 5G. One example of these bands is known as n257 [4] or 28-GHz band and goes from 26.5 to 29.5 GHz (centered at 28 GHz) showing around 10.7% bandwidth. We have set the mentioned operating frequency band as requirement for our study and experimental validation case.

The increase in the operational frequency implies some technological challenges. One of them is the reduction in the leakage between interconnected circuits due to undesired manufacturing imperfections [5]–[7]. Leakage in the interconnection of components can significantly increase the losses and generate high levels of crosstalk between adjacent elements. To reduce this leakage, a number of configurations have been proposed in the literature, such as choke flanges and corrugations [8]–[10]. Other recent works proposed the use of electromagnetic bandgap (EBG) metasurfaces created by pins, holes, or mushroom-type EBGs [11]–[18]. Holey structures are sometimes preferred due to their robustness and cost-effectiveness [19]. To increase the bandwidth of rejection of these holes, glide-symmetric metasurfaces have been recently proposed [20]–[29]. Glide symmetry is obtained by applying two geometrical operations: a reflection and a translation [30]–[32]. This concept has been recently extended to 2-D configurations [33].

In previous studies, glide-symmetric EBGs were proposed to interconnect two devices in the same technology, for example, waveguide-to-waveguide. However, in practice, it is convenient to be able to reduce the leakage directly in the transition between two different technologies. For example, active array antenna systems might include building blocks made of different materials. On one side of the system, printed circuit boards (PCBs) are required to include active components such as power amplifiers, low-noise amplifiers (LNAs), and phase shifters. This PCB with active components should be suitably interconnected and integrated with the antenna array or other passive components such as filters in the case these are not included in the PCB. Here, we propose a hybrid holey-based EBG metasurface that suppresses the leakage when having an undesired air gap in a transition between PCB and waveguide technologies. On the waveguide side, holes are drilled on the metal plate (similar to [19]). On the PCB side, substrate-integrated holes (SIHs) [34] are used. The holes on each side are located in different positions, so the complete structure mimics the behavior of holey glide-symmetric metallic EBGs [16], [17]. This novel type of unit cell is here designed to operate at the 28-GHz band, which is one of the frequency bands used for 5G deployment. It is important to remark that this design is easily scalable to higher frequencies where leakage issues become even more critical, and it constitutes a flexible solution that can be adapted to PCBs consisting of other materials used in this investigation. One relevant application of this concept is to facilitate the integration of

Manuscript received January 16, 2022; accepted February 7, 2022. Date of publication March 11, 2022; date of current version May 5, 2022. This work was supported by the Strategic Innovation Program Smarter Electronics System—a joint venture of Vinnova, Formas, and the Swedish Energy Agency, through the Project High-5 under Grant 2018-01522. *(Corresponding author: Oscar Quevedo-Teruel.)*

David González-Gallardo, Astrid Algaba-Brazález, Lars Manholm, and Martin Johansson are with Ericsson AB, 41756 Gothenburg, Sweden (e-mail: david.gonzalez.gallardo@ericsson.com; astrid.algaba.brazalez@ericsson.com; martin.n.johansson@ericsson.com; lars.manholm@ericsson.com).

Oscar Quevedo-Teruel is with the Division of Electromagnetic Engineering, KTH Royal Institute of Technology, 11428 Stockholm, Sweden (e-mail: oscarqt@kth.se).

Color versions of one or more figures in this article are available at https://doi.org/10.1109/TMTT.2022.3152731.

Digital Object Identifier 10.1109/TMTT.2022.3152731

This work is licensed under a Creative Commons Attribution 4.0 License. For more information, see https://creativecommons.org/licenses/by/4.0/

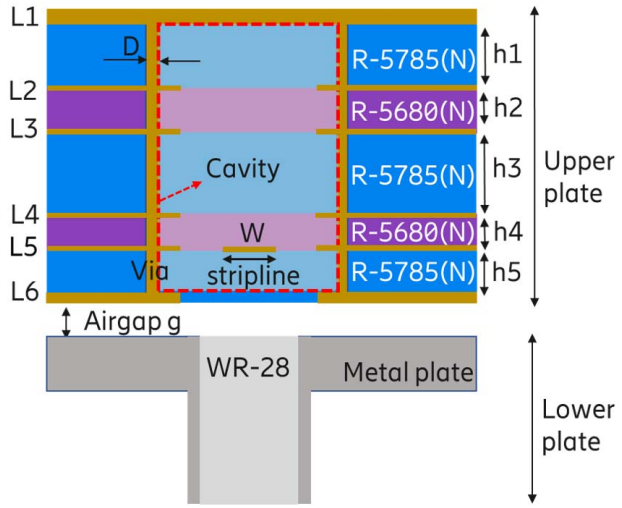

Fig. 1. Material stack-up view of the transition design for upper and lower plates.

waveguide-based filters and antennas with active components of the system which are incorporated within a multilayer PCB. To our knowledge, the only investigation previously reported and related to leakage suppression between heterogeneous interfaces (such as PCB to waveguide) is the work described in [8], which shows a very narrowband behavior and does not provide experimental evaluation.

This article is organized as follows. In Section II, we define our study case, which is a transition between PCB and a metallic waveguide. In this section, we include an analysis of the leakage with respect to an undesired air gap. Section III introduces the proposed hybrid unit cell and its operation. In Section IV, the consequences of using a truncated unit cell are analyzed. In Section V, the performance of the proposed hybrid holey-based structure is validated through simulations and measurements. Finally, in Section VI, conclusions are drawn.

II. Transition Design

To validate the operation of a hybrid unit cell, we define a realistic case in which we have a Ka-band transition from stripline (placed in a multilayer PCB) to standard WR-28 waveguide (present in a separate metallic block). This interconnection will be tested for different air gap g values with and without using metasurface to analyze leakage suppression. This transition type from stripline to rectangular waveguide using a cavity backshort embedded within the PCB is well-known and it is based on previous designs such as described in [35] and [36]. The reason to apply this transition in our investigation is to allow for a simple experimental evaluation of the hybrid glide-symmetric unit cell concept that will be described in Section III. Fig. 1 represents a cross section in which the composition of the two technologies is shown. In the top part, there is a PCB composed of five copper-coated laminates of Megtron7 R-5785(N) of permittivity $\epsilon_{r1} = 3.34$, and Prepreg R-5680(N) of permittivity $\epsilon_{r2} = 3.32$. The loss tangent of Megtron7 is 0.003. The corresponding dimensions of each copper-coated laminate are

TABLE I
Stack-Up and Main Transition Dimensions

Parameter	Value (mm)	Parameter	Value (mm)
h1	0.5	L1	0.05
h2	0.132	L2	0.018
h3	0.625	L3	0.018
h4	0.132	L4	0.018
h5	0.2	L5	0.018
D	0.3	L6	0.05
W	0.15	a	6
b	3.6	x	0.6
y	0.8		

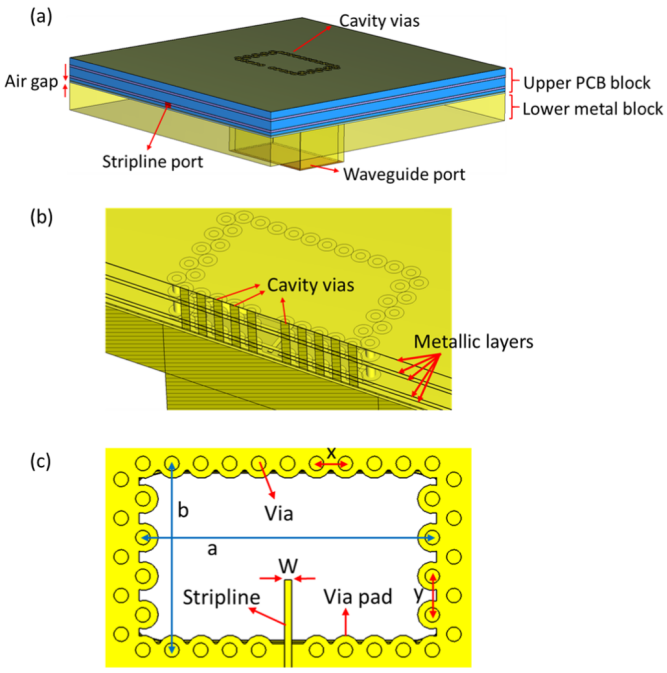

Fig. 2. PCB-to-waveguide transition under consideration. (a) Perspective view. (b) Cross section of the structure with hidden substrate layers. (c) Top view of the cavity with hidden substrate layers to visualize the stripline embedded in L5.

specified in Table I, where L1–L6 represents the thickness of each copper layer and h1–h5 denotes the thickness of each dielectric layer. In the bottom of the structure, there is an aluminum plate containing the standard WR-28. The transition consists of a dielectric-filled cavity backshort built on the multilayer PCB (see the cross section in Fig. 2 and the metallic plate containing the waveguide). The dimensions of the cavity and the via pitch in both the directions are also included in Table I and indicated in Fig. 2. Metallic vias of diameter $D = 0.3$ mm are used to set the cavity backshort boundaries. A double row of vias is used to improve shielding. The stripline is embedded within the copper layer L5 of the stack-up as shown in Fig. 1. To clarify the asymmetric stripline structure, we have depicted a sketch in Fig. 3 containing only the stripline section. The width of the line is $W = 0.15$ mm, and its corresponding characteristic impedance is $Z_o = 50\ \Omega$.

When these two technologies are attached, there might be an undesired air gap between them due to manufacturing and

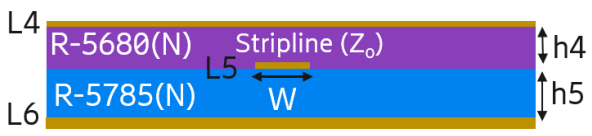

Fig. 3. Sketch of the asymmetric stripline structure.

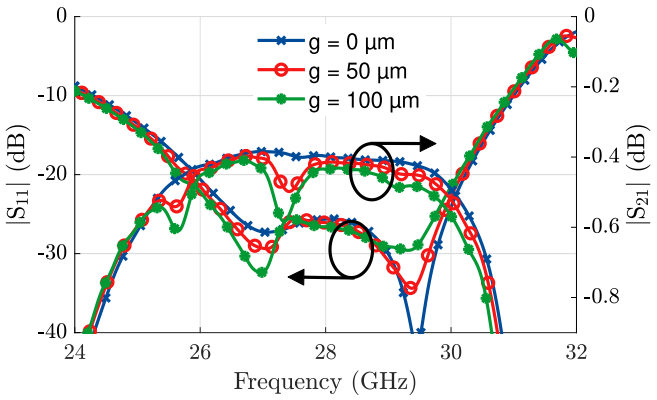

Fig. 4. *S*-parameters of the PCB-to-waveguide transition for different air gap thicknesses, g.

assembly imperfections. Due to this air gap, there is a loss of energy by means of leakage. Fig. 4 illustrates the performance of this transition in terms of reflection coefficient (S_{11}) and insertion losses (S_{21}) for different air gap thicknesses. A general requirement for this type of transition is having a S_{11} below -20 dB. Following this requirement, the bandwidth for this transition is slightly higher than 15%, which is wide enough for the allocated band for 5G. It is worth noting that although the changes in the reflection coefficient are almost negligible, the insertion loss increases for thicker air gaps. Insertion losses are composed of conductive, dielectric, and radiation losses. Therefore, any presence of radiation leakage due to larger gaps should be noticeable as a decrease in S_{21} parameter, rather than S_{11} which should be almost the same.

For testing purposes of the novel hybrid glide-symmetric unit cell, using a transition with 15% relative bandwidth has been considered enough. In Sections III and IV, it will be shown that the designed EBG structure provides a larger operating bandwidth than 15%, where leakage is reduced and the integrity of the transition performance is kept for all the gaps under investigation. It is important to point out that the transition bandwidth has not been optimized since our goal is not to achieve a wideband transition rather than obtaining a reasonable test structure to evaluate the proposed unit cell for leakage reduction. Moreover, we should not confuse the bandwidth of the transition structure with the unit cell operating bandwidth where leakage can be suppressed. The actual stopband of the hybrid unit cell will be described in terms of dispersion diagrams in Section III.

III. Unit Cell Design

In this section, we introduce first a fully metallic glide-symmetric unit cell, as it was previously proposed in [20].

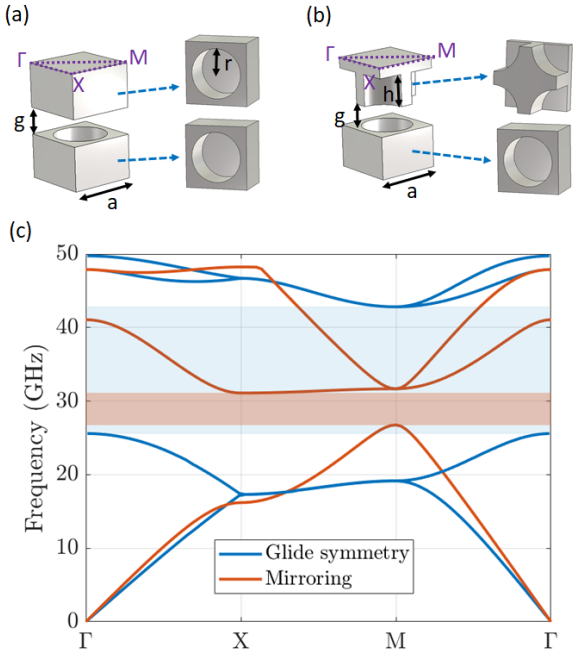

Fig. 5. Fully metallic holey configuration. (a) Schematic and irreducible Brillouin zone for a mirroring unit cell. (b) Schematic and irreducible Brillouin zone for the 2-D glide-symmetric unit cell. (c) Dispersion diagram for dimensions $a = 6$ mm, $h = 1.5$ mm, $r = 2.4$ mm, and $g = 0.1$ mm.

Then, we extend this unit cell to a hybrid version, which is compatible with a transition from PCB to metallic waveguide. To reduce the undesired leakage in the transition presented in Section II, the designed metasurface should have a stopband which covers the band from 25 to 31 GHz.

A. Fully Metallic Unit Cell

As a starting point, a fully metallic 2-D glide-symmetric holey unit cell is designed. The behavior of this type of unit cell and the effects of each one of its dimensions were deeply studied in [20] and its attenuation in [37]. A holey metallic unit cell and its glide-symmetric counterpart are illustrated in Fig. 5(a) and (b), together with irreducible Brillouin zones. Note that the irreducible Brillouin zone, denoted by symbols Γ, M, and T, makes reference to the spectral domain. Their dispersion diagrams were calculated with the eigenmode analysis of CST for each unit cell. Periodic boundary conditions were set on all the four lateral sides of the structures.

After optimization and establishing a worst case air gap scenario of $g = 0.1$ mm, the obtained dimensions for this unit cell were $a = 6$ mm, $h = 1.5$ mm, and $r = 2.4$ mm, and its dispersion diagram is illustrated in Fig. 5(c). The glide-symmetric unit cell has a wider bandwidth than the mirroring one, as previously demonstrated in the literature [20], [21]. The stopband for the glide-symmetric case exceeds the initial requirements for the transition proposed in Section II. It must be noted that in the glide-symmetric case, the stopband is not between the first and second modes (as in the conventional unit cell), but it is located between second and third instead [33].

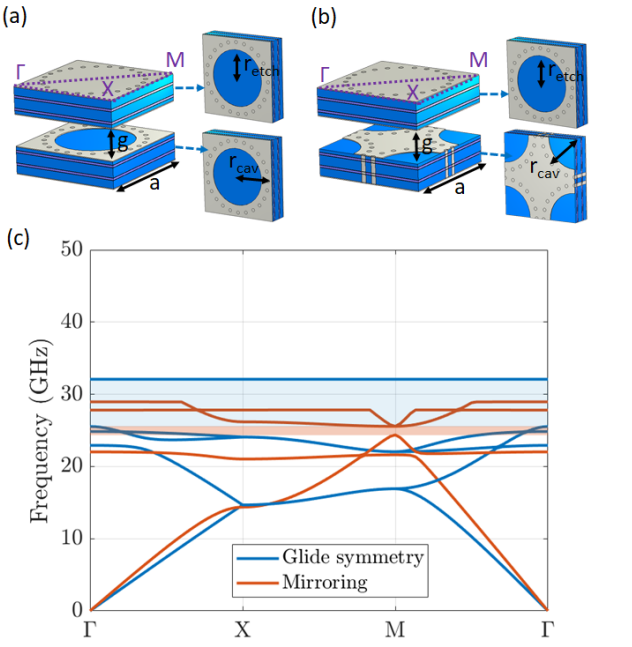

Fig. 6. SIH configuration. (a) Schematic and irreducible Brillouin zone for a mirroring unit cell. (b) Schematic and irreducible Brillouin zone for the 2-D glide-symmetric unit cell. (c) Dispersion diagram for dimensions $a = 7$ mm, $r_{\text{etch}} = 2.5$ mm, $r_{\text{cav}} = 3$ mm, and $g = 0.1$ mm.

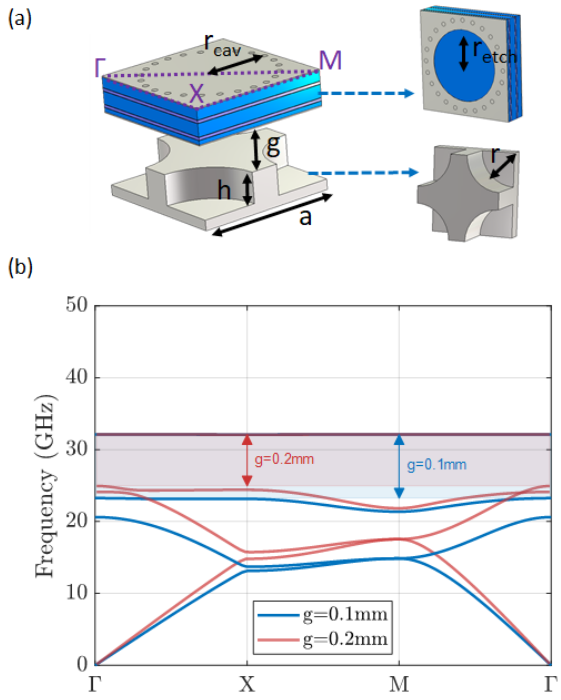

Fig. 7. Hybrid 2-D glide-symmetric holey unit cell. (a) Schematic and irreducible Brillouin zone. (b) Dispersion diagram for dimensions $a = 7$ mm, $h = 1.5$ mm, $r = 2.8$ mm, $r_{\text{etch}} = 2.5$ mm, and $r_{\text{cav}} = 3$ mm, for $g = 0.1$ mm and 0.2 mm.

B. Substrate-Integrated Holey Unit Cell

In PCB, a holey metallic configuration cannot be used. One possibility is to create holes with metallic vias attached to the top and bottom of a multilayer dielectric configuration. For a single layer, this configuration is known as SIH [34], [38], [39]. SIHs have been demonstrated to have different properties than conventional holes. In particular, in SIH, transversal electrical (TE) modes can penetrate through the vias, so the holes are electromagnetically connected. This permits differential properties in both propagation [34], [38], [39] and band rejection [40].

For a multilayer configuration, the total height of this cavity is achieved by etching the metal on each metallic layer of the PCB while its shape is obtained by placing vias around the etched holes to set its boundaries. This "etching plus vias" combination expands the possibilities of the design of the cavity by changing its shape. To keep the simplicity and a structure similar to the already existing ones, we chose here a circular cylindrical cavity which mimics the behavior of a drilled hole for small heights of the holes [40]. This unit cell is illustrated in Fig. 6(a) and (b) for mirroring and glide symmetry.

After an optimization process, the obtained dimensions for this unit cell are $a = 7$ mm, $r_{\text{etch}} = 2.5$ mm, and $r_{\text{cav}} = 3$ mm for a worst case scenario of $g = 0.1$ mm. The dispersion diagram of these unit cells is plotted in Fig. 6(c). The glide-symmetric case has a broader bandwidth of rejection. However, its bandwidth is narrower than in the case of the fully metallic configuration proposed in the previous section.

C. Hybrid Unit Cell

As stated previously, a fully metallic unit cell cannot be directly integrated in PCB. For the transition illustrated in Fig. 2, a hybrid unit cell is needed. On the waveguide side, we can keep a fully metallic configuration as in the previous design, while on the PCB side, we use an SIH structure as described in the previous section.

The new unit cell is illustrated in Fig. 7(a) together with its irreducible Brillouin zone. This unit cell does not possess glide symmetry since it is not invariant after translation and mirroring [33]. Two new parameters must be designed for this hybrid structure: the radius of the etched metal (r_{etch}) and the radius of the ring of vias (r_{cav}). After an optimization process, the obtained dimensions are $a = 7$ mm, $h = 1.5$ mm, $r = 2.8$ mm, $r_{\text{etch}} = 2.5$ mm, and $r_{\text{cav}} = 3$ mm for a worst case scenario of $g = 0.1$ mm. The dispersion diagram of this unit cell is plotted in Fig. 7(b), together with the case of $g = 0.2$ mm, demonstrating that the unit cell is robust to even larger air gaps. Since there is no glide symmetry, there is a narrow stopband between the first and second modes for the on-axis propagation, and a third mode appears, which limits the bandwidth of the stopband. The chosen stopband is between the third and fourth modes since it provides enough bandwidth for the transition proposed in Section II. The width of this stopband is narrower than in the fully metallic case, although wider than in the case of glide-symmetric SIH due to the influence of the fully metallic configuration in one of the sides. In any case, it satisfies the initial requirements for the proposed transition.

IV. Truncated Unit Cell

The results in Section III-C demonstrate the effectiveness of the hybrid unit cell as an EBG. Now, we aim at using

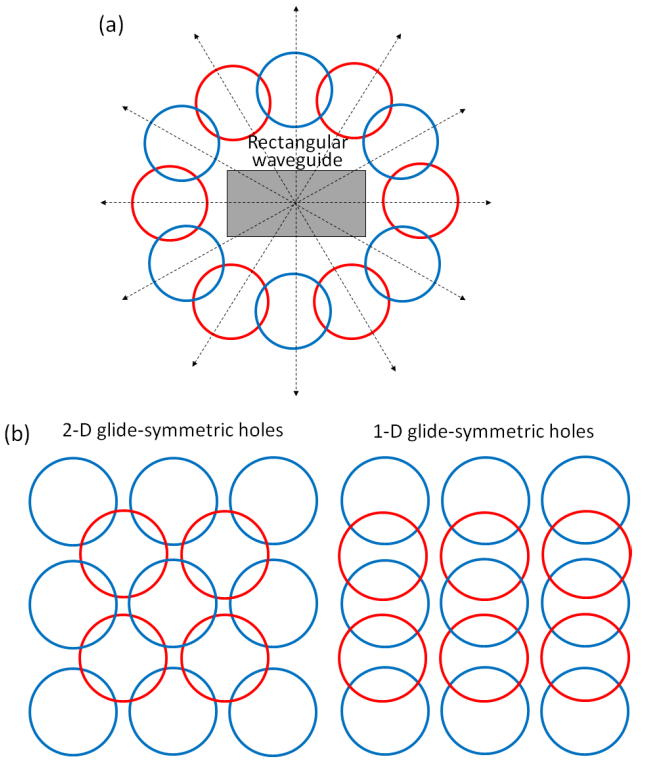

Fig. 8. (a) Unit cells placed on a circular topology around the transition and (b) comparison between 2-D and 1-D glide-symmetric configurations. Red and blue circles represent two different layers (top and bottom).

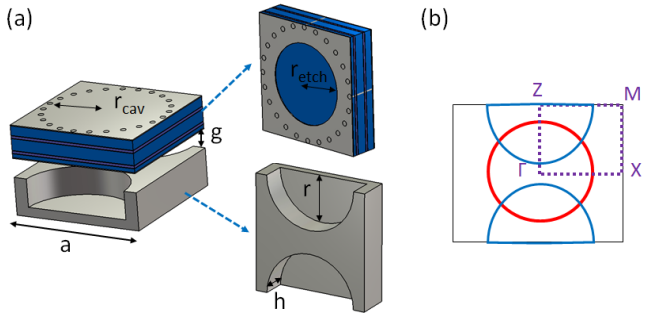

Fig. 9. (a) Hybrid 1-D glide-symmetric holey unit cell and (b) irreducible Brillouin zone of the 1-D glide-symmetric structure.

this hybrid unit cell to suppress the leakage in the transition described in Section II with a configuration as the one illustrated in Fig. 8(a).

To produce a compact configuration, only one tier of unit cells is placed around the transition. This configuration was previously proposed for fully metallic transitions [16]. Although the 2-D glide-symmetric unit cell was useful to understand the overall performance of this hybrid topology, in this compact scenario, a 1-D glide-symmetric unit cell is closer to the real configuration. In Fig. 8(b), we illustrate the differences between 1-D and 2-D configurations.

We made two assumptions regarding the circular topology model.

1) The proximity between transition and metasurface allows us to assume that the leakage propagation follows a cylindrical wave model. For this reason, all the unit cells of the ring are considered as equal.
2) The leakage propagates through the unit cells following the path from Γ to X, in which the phase does not change transversally. Therefore, avoiding the propagation in this region of the dispersion diagram is enough for this specific configuration.

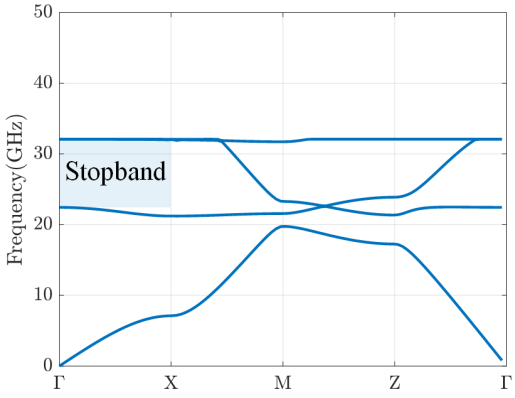

Fig. 10. Dispersion diagram for the 2-D hybrid glide-symmetric holey structure with dimensions: $a = 7$ mm, $h = 1.5$ mm, $r = 2.8$ mm, $r_{etch} = 2.5$ mm, $r_{cav} = 3$ mm, and $g = 0.1$ mm.

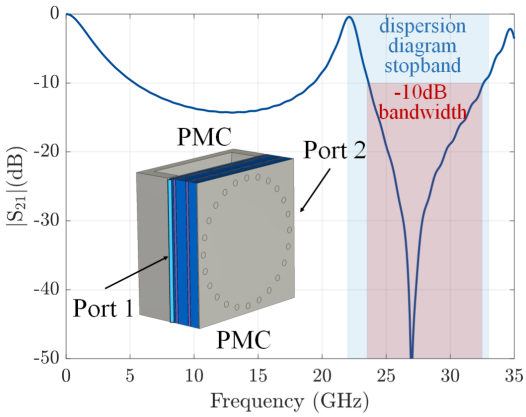

Fig. 11. Insertion losses of a unit cell when excited with two waveguide ports and perfect magnetic conditions are imposed on both sides. In shaded blue, the stopband from the dispersion diagram in Fig. 10 is highlighted. In shaded red, the −10-dB bandwidth is indicated.

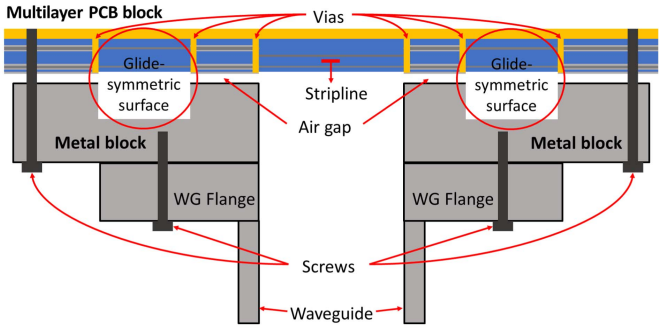

Fig. 12. Cross section view of the transition and the surrounding metasurface. A metal block is used to drill the holes of the lower plate and it is screwed to the standard waveguide flange.

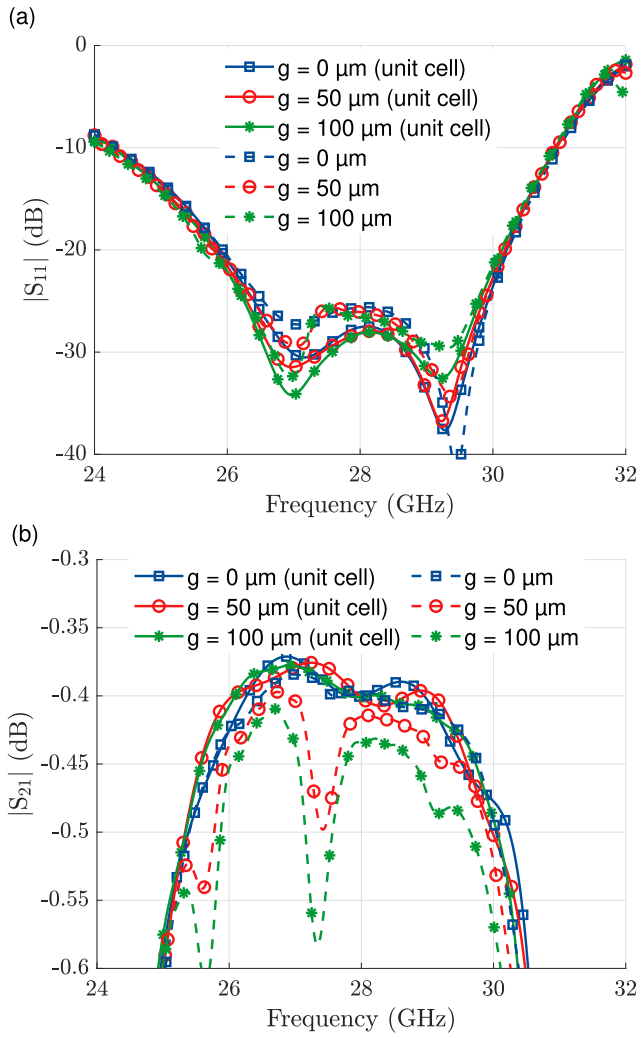

Fig. 13. Simulated S-parameters of the single transition for different air gap thicknesses in the absence/presence of the hybrid unit cells: (a) $|S_{11}|$ and (b) $|S_{21}|$.

The 1-D hybrid glide-symmetric holey unit cell and its irreducible Brillouin zone are shown in Fig. 9. Note that the change from 2-D to 1-D glide symmetry implies a change in the shape of the irreducible Brillouin zone of the unit cell. After an optimization for an air gap of $g = 0.1$ mm, the obtained dimensions were: $a = 7$ mm, $h = 1.5$ mm, and $r = 2.8$ mm, $r_{\text{etch}} = 2.5$ mm, and $r_{\text{cav}} = 3$ mm. The dispersion diagram for this unit cell is plotted in Fig. 10. Some differences with respect to the previous dispersion diagram can be noted. Here, we must focus only on the first region of the dispersion diagram (Γ to X), and a stopband between the second and third modes can be observed at the frequencies of interest.

V. Leakage Reduction

In Sections III and IV, a hybrid unit cell that presents a stopband for the required bandwidth was designed. Here, we combine this unit cell with the transition, and we evaluate the insertion losses.

A. Single Transition

Fig. 12 illustrates a cross section view of the whole structure (transition and surrounding metasurface). Several air gap thicknesses were simulated and compared in the absence/presence of the hybrid unit cells for a single transition. The results of the reflection coefficient and the insertion loss are plotted

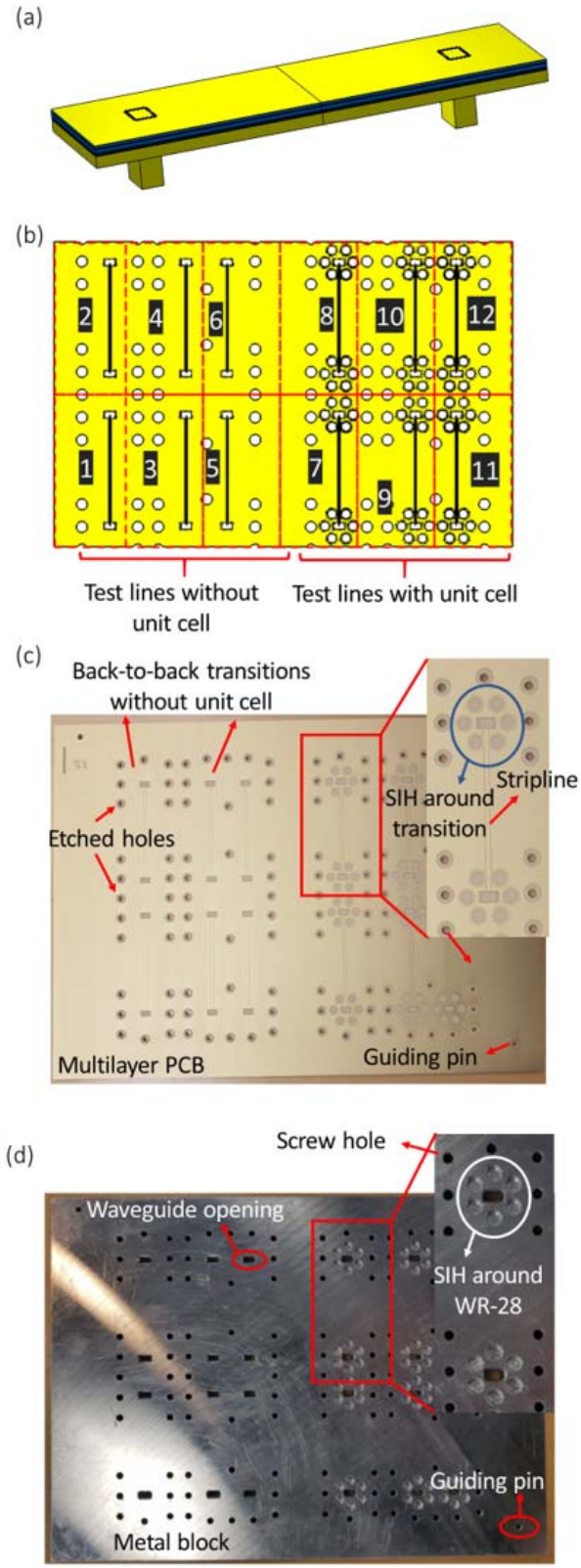

Fig. 14. (a) Back-to-back transition, (b) top view of the second metal layer of the PCB (enumerating each of the transitions), (c) top view of the manufactured multilayer PCB, and (d) top view of the manufactured metal block including waveguide openings.

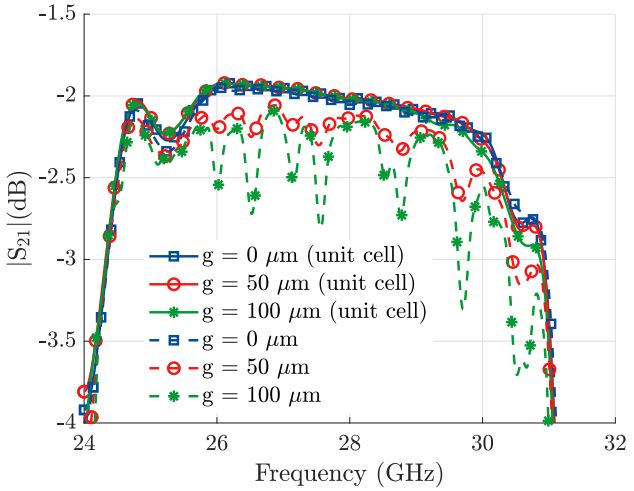

Fig. 15. Simulated $|S_{21}|$ of the back-to-back transition for different air gap thicknesses in the absence/presence of the hybrid unit cells.

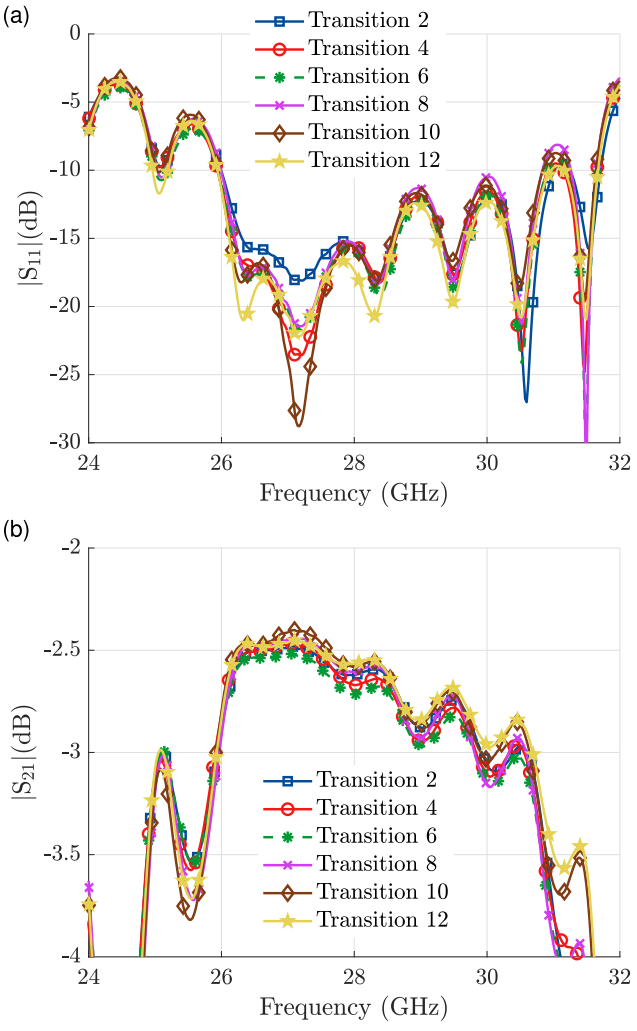

Fig. 16. Measured S-parameters in transitions 2, 4, 6, 8, 10, and 12 [see Fig. 14(d)] with $g = 0$ μm: (a) $|S_{11}|$ and (b) $|S_{21}|$.

in Fig. 13. Based on these results, the effect of adding hybrid unit cells is negligible in terms of reflection coefficient since the bandwidth stays almost constant. On the other hand, the insertion loss remains constant regardless of the thickness of the air gap after the addition of the hybrid unit cells. The very small additional insertion losses are due to the reduced amount of leakage (and propagation between plates), thanks to the bandgap nature of the hybrid unit cell.

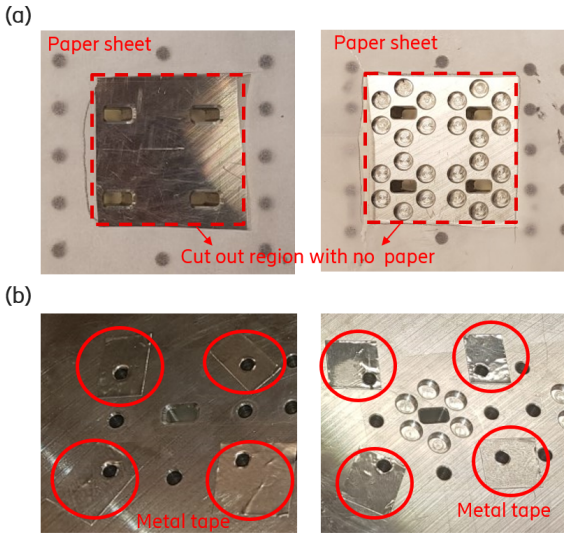

Fig. 17. Creation of the gaps for experimental evaluation. (a) 30-μm paper sheet placement (around waveguides without metasurface and with metasurface). (b) 65-μm metallic tape location around screw holes.

These conclusions prove the correct behavior of the designed hybrid unit cell. Having an air gap of up to 100 μm gives negligible impact in terms of leakage, making the transition very robust. Additionally, the connection between printed board and waveguide can be done with screws instead of using more expensive methods, such as galvanic contact, which are aimed to avoid undesired air gaps in the transition.

B. Back-to-Back Transition

With one transition, it is possible to assess the viability of the proposed hybrid unit cell. However, this simple configuration is difficult to measure with a prototype. Therefore, a waveguide–PCB–waveguide transition was designed and manufactured as illustrated in Fig. 14(a).

The prototype consists of two parts, the PCB shown in Fig. 14(c) and a metal block in Fig. 14(d). Several back-to-back transitions were placed to study the crosstalk for both the E- and H-planes. The full prototype has areas with and without unit cells, as illustrated in Fig. 14(b). Therefore, with this prototype, it is possible to determine the effect of unit cells over the performance of the device.

Fig. 15 shows the simulated insertion losses of the back-to-back transition in the absence/presence of the hybrid unit cells. Losses are higher (2.1 dB) than for a single transition (0.4 dB). Note that this configuration does not only include two transitions but also a 6-cm length (10λ) stripline between them with an estimated dielectric plus conductor losses of around 0.25 dB/cm.

With the aim to assess the repeatability of the results, different transitions, named 2, 4, 6, 8, 10, and 12 [see Fig. 14(b)],

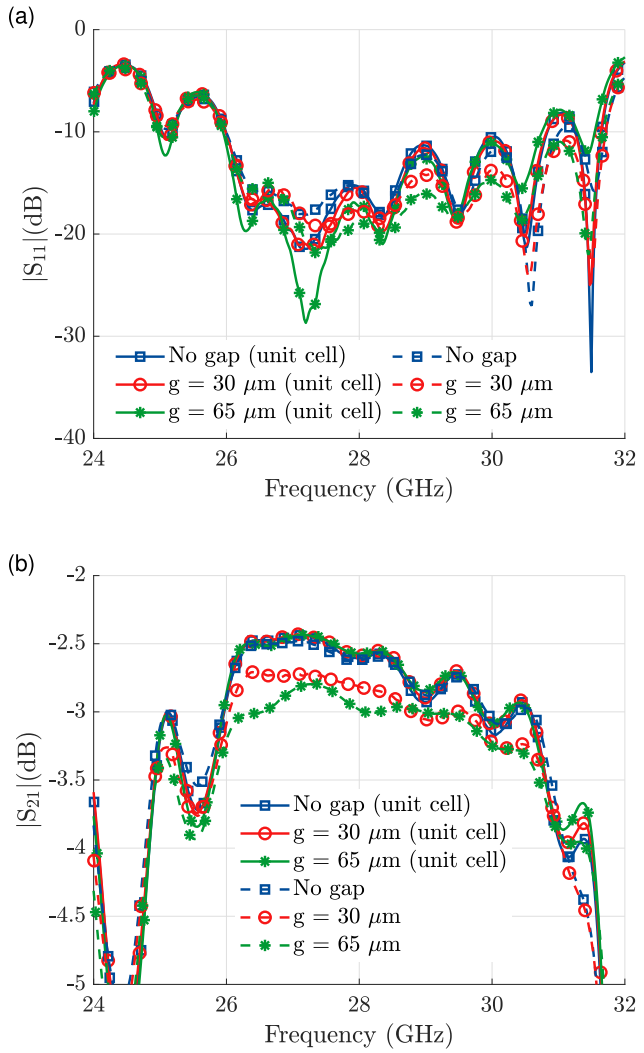

Fig. 18. Measured S-parameters of a back-to-back transition for different air gap thicknesses in the absence/presence of the hybrid unit cells. The measured configurations correspond to numbers 2 and 8 of Fig. 14(b): (a) $|S_{11}|$ and (b) $|S_{21}|$.

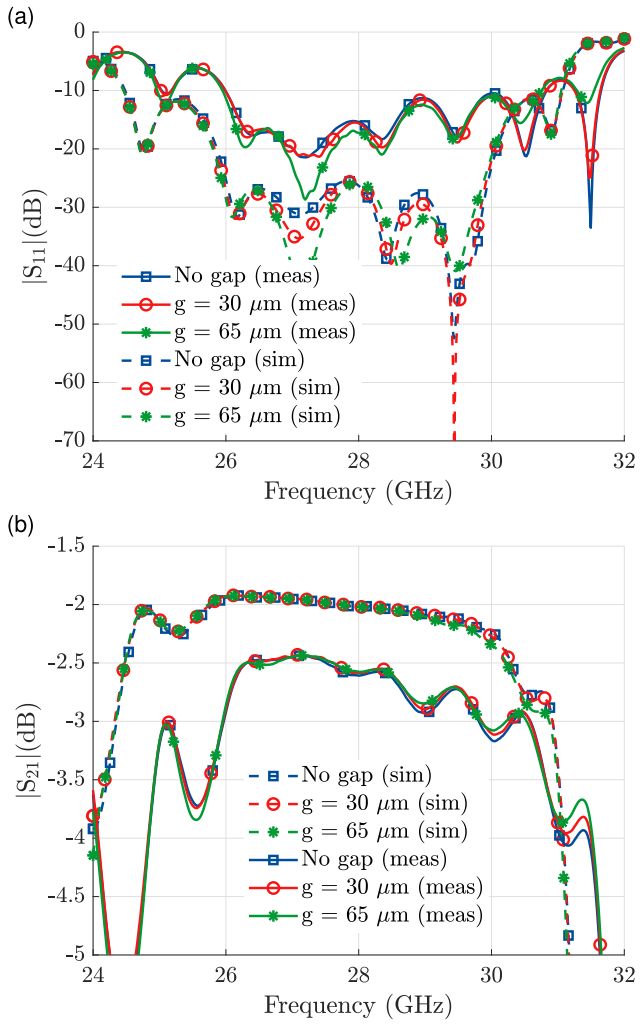

Fig. 19. S-parameters' comparison between simulations and measurements of the back-to-back transition including the hybrid unit cells: (a) $|S_{11}|$ and (b) $|S_{21}|$.

were measured with nominally no air gap between layers. The S-parameters of these measurements are illustrated in Fig. 16. Although the performance of each transition varies slightly due to nonuniform placing of the surrounding screws, their general behavior is similar. In the case of having no air gap, the presence of the unit cell is negligible in terms of reflection coefficient and insertion losses.

To study the effect of an undesirable air gap, two artificial layers of different thicknesses were placed between both the plates: a paper sheet of 30 μm and a metallic tape of 65 μm. The 30-μm paper sheet is fixed on the top of the metallic block, and certain paper regions are removed around the transitions and metasurfaces to create the gap, as shown in Fig. 17(a). The 65-μm metallic tape is placed around the screw holes as illustrated in Fig. 17(b).

The back-to-back transition was measured, and the results are shown in Fig. 18. The measured configurations correspond to numbers 2 and 8 of Fig. 14(b). The effect of having an air gap is significant for the case of no hybrid unit cell. However, there are only small differences with the use of the hybrid unit cell, demonstrating its effectiveness in suppressing the leakage.

These results are consistent with the simulations obtained in Sections III and IV. Fig. 19 shows the comparison in terms of reflection coefficient and insertion losses between simulations and measurements of the back-to-back transition with and without the hybrid unit cells. The measurements are similar for different gaps despite that the prototype was reassembled for each measurement. This demonstrates the robustness offered by the hybrid unit cells. The reflection coefficient of the prototype is below -10 dB for the desired bandwidth. The measurement results have a slightly worse performance than in simulations. The reason for this discrepancy is possibly mainly due to PCB manufacturing tolerances. It has been seen in simulations that the used transition design is sensitive to the variations in the dielectric thickness of the multilayer PCB. According to the PCB manufacturer, an approximate tolerance of $\pm 7\%$ in the laminate and prepreg layers of Megtron 7 could be expected. A tolerance analysis of the total PCB thickness was carried out to understand the effect of such dielectric variation, and it was seen that a variation of ± 0.1 mm in the total PCB thickness would have an impact similar to the observed in our measurements. Also, a small frequency

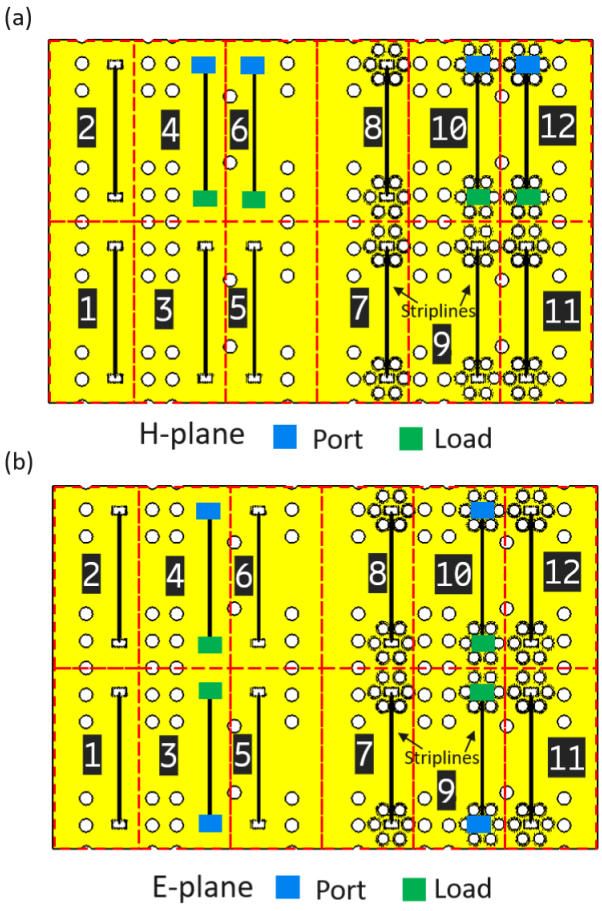

Fig. 20. Position of the ports and the loads for the H-plane and E-plane crosstalk study. (a) H-plane crosstalk. (b) E-plane crosstalk.

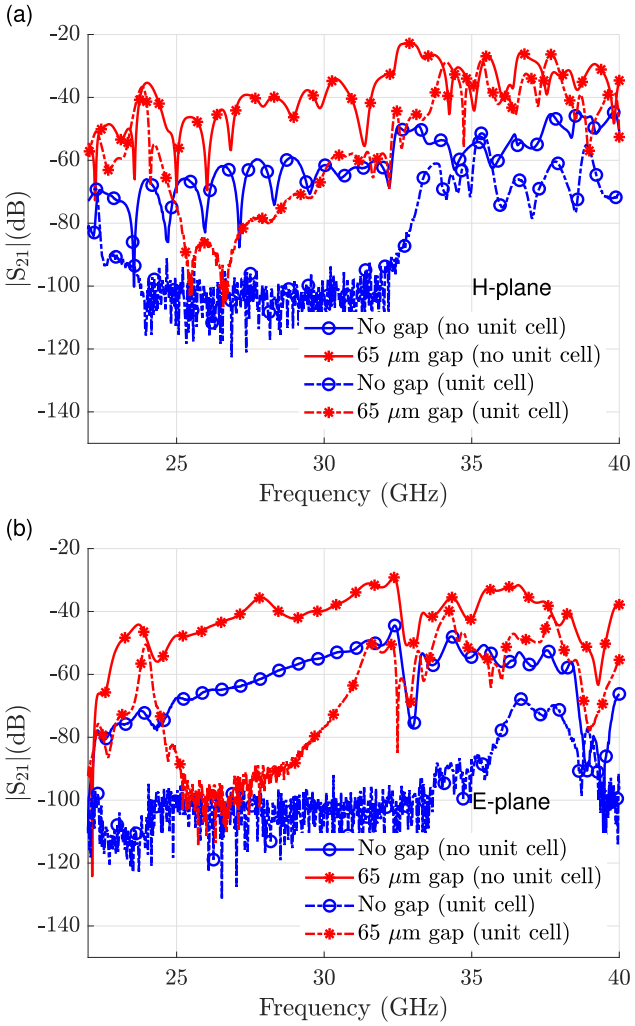

Fig. 21. Measured crosstalk in the absence/presence of hybrid unit cells for 65-μm air gap and nonenforced air gap, named as "no gap." (a) H-plane. (b) E-plane.

shift can be noted. The most probable reason for this shift is a slight lateral misalignment between PCB and metal plate when they were screwed together. This was also proved by carrying out a simulation considering a lateral misalignment in the design up to 0.3 mm. The complete tolerance analysis of the designed structure is reported in [41]. Nevertheless, the purpose of this work is not to demonstrate a perfect transition performance rather than to prove that we can reduce potential leakage in PCB-to-waveguide interconnects when using a hybrid glide-symmetric unit cell.

Finally, a study of the crosstalk was carried out. Two waveguide ports and two matched loads were placed on different back-to-back transitions, and the effect of hybrid unit cells was studied. Fig. 20 shows the selected position of the loads and the ports to study two scenarios: H-plane and E-plane crosstalk.

The results of this study are plotted in Fig. 21. The effect of the hybrid unit cells is clearly noted in the insertion losses. For a 65-μm air gap, the crosstalk is much lower for the case of using hybrid unit cells. It is important to remark that the results presented in Fig. 21 and denoted as "no gap" refer to the case in which no air gap is enforced. However, due to the imperfections in the setup and manufacturing, there is a gap between layers which cannot be easily measured or quantified. The hybrid unit cell also reduces the crosstalk in this "no gap" scenario.

VI. Conclusion

Here, we proposed a novel hybrid glide-symmetric unit cell (PCB and fully metallic) for leakage reduction in the presence of undesired gaps in PCB-to-waveguide interconnects. The experimental proof of concept has been realized via a simple test structure based on a stripline-to-waveguide transition operating at the Ka-band. The unit cell is used to generate a metasurface with a stopband that goes from 22 to 33 GHz, i.e., 40% relative bandwidth, which is placed around a PCB-to-waveguide cavity backshort transition. The unit cell is designed with mimicked glide-symmetric holes. The use of PCB technology opens new possibilities for alternative shapes and material compositions. The leakage remains negligible for gaps up to 65 μm. Therefore, the use of simple screws instead of more complex fixed attaching methods, like galvanic contact or glue, is possible. A set of back-to-back test transitions are simulated, and a prototype was manufactured with the absence/presence of the hybrid unit cell. Both simulations

and measurements demonstrate the feasibility of the design, although a small increase in the insertion losses was obtained in the measurements. Crosstalk was also studied, demonstrating reduced levels with the use of hybrid unit cells. It is important to remark that the proposed unit cell is easily scalable to higher frequencies where the leakage problem in hybrid interconnections becomes much more critical. Moreover, this EBG structure is not limited to one specific dielectric stack-up, and it can be adapted to different materials. The here-presented concept of hybrid glide-symmetric unit cell has been protected by a patent application [42].

REFERENCES

[1] A. Osseiran, S. Parkvall, P. Persson, A. Zaidi, S. Magnusson, and K. Balachandran. (Apr. 2020). *5G Wireless Access: An Overview*. Accessed: May 2021. [Online]. Available: https://www.ericsson.com/en/reports-and-papers/white-papers/5g-wireless% -access-an-overview.

[2] G. Wikström *et al.*, (Nov. 2020). *Ever-Present Intelligent Communication*. Accessed: May 2021. [Online]. Available: https://www.ericsson.com/en/reports-and-papers/white-papers/a-research-% outlook-towards-6g

[3] (Oct. 2020). *Ericsson Microwave Outlook*. Ericsson AB, White Paper. [Online]. Available: https://www.ericsson.com/4a811d/assets/local/reports-papers/microwave-% outlook/2020/2020-ericsson-microwave-outlook-report-digital.pdf

[4] 3GPP. *Technical Specification TS38.104, Release 17 (version 17.2.0)*. Accessed: Jul. 2021. [Online]. Available: https://portal.3gpp.org/desktopmodules/Specifications/SpecificationDetails.aspx?specificationId=3202

[5] K. Seo, "Planar microstrip-to-waveguide transition in millimeter-wave band," in *Advancement in Microstrip Antennas With Recent Applications*. London, U.K.: IntechOpen, 2013.

[6] A. Ariffin, D. Isa, and A. Malekmohammadi, "Broadband transition from microstrip line to waveguide using a radial probe and extended GND planes for millimeter wave applications," *Prog. Electromagn. Res. Lett.*, vol. 60, pp. 95–100, 2016.

[7] G. Lischka, "Design and realization of microstrip transitions up to 90 GHz," M.S. thesis, Inst. Nachrichtentechnik Hochfrequenztechnik, Technischen Univ. Wien, Vienna, Austria, 2005.

[8] Y. Mizuno, K. Sakakibara, and N. Kikuma, "Loss reduction of microstrip-to-waveguide transition suppressing leakage from gap between substrate and waveguide by choke structure," in *Proc. Int. Symp. Antennas Propag. (ISAP)*, Oct. 2016, pp. 374–375.

[9] B. Pyne, R. Naruse, H. Saito, J. Hirokawa, V. Ravindra, and P. R. Akbar, "Robust contactless noncircular choke flange for wideband waveguide applications," *IEEE Trans. Microw. Theory Techn.*, vol. 67, no. 3, pp. 861–867, Mar. 2019.

[10] V. Buiculescu and A. Ştefănescu, "Choke flange-like structure for direct connection of cascaded substrate integrated waveguide components," *Electron. Lett.*, vol. 48, no. 21, pp. 1349–1350, Oct. 2012.

[11] E. Pucci and P.-S. Kildal, "Contactless non-leaking waveguide flange realized by bed of nails for millimeter wave applications," in *Proc. 6th Eur. Conf. Antennas Propag. (EUCAP)*, Mar. 2012, pp. 3533–3536.

[12] S. Rahiminejad, E. Pucci, V. Vassilev, P.-S. Kildal, S. Haasl, and P. Enoksson, "Polymer gap adapter for contactless, robust, and fast measurements at 220–325 GHz," *J. Microelectromech. Syst.*, vol. 25, no. 1, pp. 160–169, Feb. 2016.

[13] D. Sun, Z. Chen, C. Yao, and J. Xu, "Flexible rectangular waveguide based on cylindrical contactless flange," *Electron. Lett.*, vol. 52, no. 25, pp. 2042–2044, Dec. 2016.

[14] D. Sun and J. Xu, "Real time rotatable waveguide twist using contactless stacked air-gapped waveguides," *IEEE Microw. Wireless Compon. Lett.*, vol. 27, no. 3, pp. 215–217, Mar. 2017.

[15] X. Chen, D. Sun, W. Cui, and Y. He, "A folded contactless waveguide flange for low passive-intermodulation applications," *IEEE Microw. Wireless Compon. Lett.*, vol. 28, no. 10, pp. 864–866, Oct. 2018.

[16] M. Ebrahimpouri, A. A. Brazalez, L. Manholm, and O. Quevedo-Teruel, "Using glide-symmetric holes to reduce leakage between waveguide flanges," *IEEE Microw. Wireless Compon. Lett.*, vol. 28, no. 6, pp. 473–475, Jun. 2018.

[17] Z. S. He, S. An, J. Liu, and C. Jin, "Variable high precision wide D-band phase shifter," *IEEE Access*, vol. 8, pp. 140438–140444, 2020.

[18] Z. S. He, A. Hassona, A. Perez-Ortega, and H. Zirath, "A compact PCB gasket for waveguide leakage suppression at 110–170 GHz," in *IEEE MTT-S Int. Microw. Symp. Dig.*, Aug. 2020, pp. 888–891.

[19] D. Dawn, Y. Ohashi, and T. Shimura, "A novel electromagnetic bandgap metal plate for parallel plate mode suppression in shielded structures," *IEEE Microw. Wireless Compon. Lett.*, vol. 12, no. 5, pp. 166–168, May 2002.

[20] M. Ebrahimpouri, O. Quevedo-Teruel, and E. Rajo-Iglesias, "Design guidelines for gap waveguide technology based on glide-symmetric holey structures," *IEEE Microw. Wireless Compon. Lett.*, vol. 27, no. 6, pp. 542–544, Jun. 2017.

[21] M. Ebrahimpouri, E. Rajo-Iglesias, Z. Sipus, and O. Quevedo-Teruel, "Cost-effective gap waveguide technology based on glide-symmetric holey EBG structures," *IEEE Trans. Microw. Theory Techn.*, vol. 66, no. 2, pp. 927–934, Feb. 2018.

[22] E. Rajo-Iglesias, M. Ebrahimpouri, and O. Quevedo-Teruel, "Wideband phase shifter in groove gap waveguide technology implemented with glide-symmetric holey EBG," *IEEE Microw. Wireless Compon. Lett.*, vol. 28, no. 6, pp. 476–478, Jun. 2018.

[23] Q. Liao, E. Rajo-Iglesias, and O. Quevedo-Teruel, "Ka-band fully metallic TE_{40} slot array antenna with glide-symmetric gap waveguide technology," *IEEE Trans. Antennas Propag.*, vol. 67, no. 10, pp. 6410–6418, Oct. 2019.

[24] P. Padilla, Á. Palomares-Caballero, A. Alex-Amor, J. Valenzuela-Valdés, J. M. Fernández-González, and O. Quevedo-Teruel, "Broken glide-symmetric holey structures for bandgap selection in gap-waveguide technology," *IEEE Microw. Wireless Compon. Lett.*, vol. 29, no. 5, pp. 327–329, May 2019.

[25] A. Monje-Real, N. J. G. Fonseca, O. Zetterstrom, E. Pucci, and O. Quevedo-Teruel, "Holey glide-symmetric filters for 5G at millimeter-wave frequencies," *IEEE Microw. Wireless Compon. Lett.*, vol. 30, no. 1, pp. 31–34, Jan. 2020.

[26] O. Zetterstrom, E. Pucci, P. Padilla, L. Wang, and O. Quevedo-Teruel, "Low-dispersive leaky-wave antennas for mmWave point-to-point high-throughput communications," *IEEE Trans. Antennas Propag.*, vol. 68, no. 3, pp. 1322–1331, Mar. 2020.

[27] Q. Chen, O. Zetterstrom, E. Pucci, A. Palomares-Caballero, P. Padilla, and O. Quevedo-Teruel, "Glide-symmetric holey leaky-wave antenna with low dispersion for 60 GHz point-to-point communications," *IEEE Trans. Antennas Propag.*, vol. 68, no. 3, pp. 1925–1936, Mar. 2020.

[28] Á. Palomares-Caballero, A. Alex-Amor, P. Padilla, and J. F. Valenzuela-Valdés, "Dispersion and filtering properties of rectangular waveguides loaded with holey structures," *IEEE Trans. Microw. Theory Techn.*, vol. 68, no. 12, pp. 5132–5144, Dec. 2020.

[29] A. Palomares-Caballero, A. Alex-Amor, J. Valenzuela-Valdes, and P. Padilla, "Millimeter-wave 3-D-printed antenna array based on gap-waveguide technology and split E-plane waveguide," *IEEE Trans. Antennas Propag.*, vol. 69, no. 1, pp. 164–172, Jan. 2021.

[30] P. J. Crepeau and P. R. McIsaac, "Consequences of symmetry in periodic structures," *Proc. IEEE*, vol. 52, no. 1, pp. 33–43, Jan. 1964.

[31] R. B. Kieburtz and J. Impagliazzo, "Multimode propagation on radiating traveling-wave structures with glide-symmetric excitation," *IEEE Trans. Antennas Propag.*, vol. AP-18, no. 1, pp. 3–7, Jan. 1970.

[32] A. Hessel, M. H. Chen, R. C. M. Li, and A. A. Oliner, "Propagation in periodically loaded waveguides with higher symmetries," *Proc. IEEE*, vol. 61, no. 2, pp. 183–195, Feb. 1973.

[33] O. Quevedo-Teruel, Q. Chen, F. Mesa, N. J. G. Fonseca, and G. Valerio, "On the benefits of glide symmetries for microwave devices," *IEEE J. Microw.*, vol. 1, no. 1, pp. 457–469, Jan. 2021.

[34] Q. Chen, F. Mesa, P. Padilla, X. Yin, and O. Quevedo-Teruel, "Efficient leaky-lens antenna at 60 GHz based on a substrate-integrated-holey metasurface," *IEEE Trans. Antennas Propag.*, vol. 68, no. 12, pp. 7777–7784, Dec. 2020.

[35] R. Głogowski, J.-F. Zürcher, C. Peixeiro, and J. R. Mosig, "Ka-band rectangular waveguide to suspended stripline transition," *IEEE Microw. Wireless Compon. Lett.*, vol. 23, no. 11, pp. 575–577, Nov. 2013.

[36] Y. Deguchi, K. Sakakibara, N. Kikuma, and H. Hirayama, "Millimeter-wave microstrip-to-waveguide transition operating over broad frequency bandwidth," in *IEEE MTT-S Int. Microw. Symp. Dig.*, Jun. 2005, pp. 2107–2110.

[37] Q. Chen, F. Mesa, X. Yin, and O. Quevedo-Teruel, "Accurate characterization and design guidelines of glide-symmetric holey EBG," *IEEE Trans. Microw. Theory Techn.*, vol. 68, no. 12, pp. 4984–4994, Dec. 2020.

[38] O. Zetterstrom, R. Hamarneh, and O. Quevedo-Teruel, "Experimental validation of a metasurface Luneburg lens antenna implemented with glide-symmetric substrate-integrated holes," *IEEE Antennas Wireless Propag. Lett.*, vol. 20, no. 5, pp. 698–702, May 2021.
[39] Q. Chen, F. Giusti, G. Valerio, F. Mesa, and O. Quevedo-Teruel, "Anisotropic glide-symmetric substrate-integrated-holey metasurface for a compressed ultrawideband Luneburg lens," *Appl. Phys. Lett.*, vol. 118, no. 8, Feb. 2021, Art. no. 084102.
[40] F. Ghasemifard, F. Mesa, G. Valerio, and O. Quevedo-Teruel, "Propagation characteristics in substrate integrated holey metasurfaces," in *Proc. 14th Eur. Conf. Antennas Propag. (EuCAP)*, Mar. 2020, pp. 1–4.
[41] D. González-Gallardo, "Leakage suppression for PCB-waveguide interconnects using hybrid metasurfaces," M.S. thesis, Dept. Elect. Eng., KTH Roy. Inst. Technol., Stockholm, Sweden, 2019.
[42] "A metasurface arrangement," European Patent Appl. 2019/055 189, 2019.

David González-Gallardo received the Telecommunication Engineering degree from the University of Jaén, Jaén, Spain, in 2016, the Master of Telecommunication Engineering degree from the Polytechnic University of Catalonia, Barcelona, Spain, in 2019, and the M.Sc. degree in engineering from the KTH Royal Institute of Technology of Stockholm, Stockholm, Sweden, in 2019.

He worked as a Radar Systems Engineer and a Technical Leader of Long Range Fixed and Non-Fixed Radars. He currently works as an Antenna Design Engineer with the Product Development Unit, Ericsson, Gothenburg, Sweden. His research interests are millimeter-wave antennas for 5G and radar appplications, microwave passive components, radome design, and metasurfaces.

Astrid Algaba-Brazález received the Telecommunication Engineering degree from the Miguel Hernández University of Elche, Alicante, Spain, in 2009, and the Licentiate of Engineering and Ph.D. degrees from the Chalmers University of Technology, Gothenburg, Sweden, in 2013 and 2015, respectively.

She joined Ericsson Research, Gothenburg, in November 2014, where she currently works as a Senior Researcher with the Antenna and Microwave Hardware Unit with special focus on 5G and 6G antenna hardware activities. She has also been leading all research activities related to metasurfaces within Ericsson Research since 2015. Her research interests include millimeter and submillimeter antenna array technologies, lens antennas, design of microwave passive components such as filters, metasurfaces, integration of active components and antennas at millimeter-wave frequencies, and design of interconnects and transitions to achieve such integration.

Dr. Algaba-Brazález was a recipient of the second Best Paper Award at the International Symposium on Antennas and Propagation (ISAP) held in 2017 and the Best Paper Award in Antennas at the European Conference on Antennas and Propagation (EuCAP) held in 2020.

Lars Manholm received the M.Sc. degree in electrical engineering and the Licentiate of Technology degree in electromagnetics from the Chalmers University of Technology, Gothenburg, Sweden, in 1994 and in 1998, respectively.

He joined Ericsson Microwave Systems, Gothenburg, as an Antenna Designer, in 1998, and Ericsson Research, Gothenburg, in 2003, where he holds a position as a Master Researcher in antenna hardware. His research interests include electronically steerable antennas and antenna arrays for cellular base station and fixed radio link applications at microwave and millimeter-wave frequencies.

Martin Johansson (Senior Member, IEEE) received the M.Sc. degree in engineering physics and the Ph.D. degree in electromagnetics from the Chalmers University of Technology, Gothenburg, Sweden, in 1986 and 1997, respectively.

He joined Ericsson Research, Ericsson AB, Gothenburg, in 1997, where he currently serves as an Expert in antenna technology. His current research interests include antenna technology for mobile communications, antenna system modeling, and deterministic channel modeling.

Oscar Quevedo-Teruel (Senior Member, IEEE) received the Telecommunication Engineering and Ph.D. degrees from the Carlos III University of Madrid, Spain, in 2005 and 2010, respectively.

From 2010 to 2011, he joined the Department of Theoretical Physics of Condensed Matter, Universidad Autonoma de Madrid, Madrid, Spain, as a Research Fellow and went on to continue his Post-Doctoral Research with the Queen Mary University of London, London, U.K., from 2011 to 2013. In 2014, he joined the Division of Electromagnetic Engineering, School of Electrical Engineering and Computer Science, KTH Royal Institute of Technology, Stockholm, Sweden, where he is a Professor and the Director of the Master Programme in Electromagnetics Fusion and Space Engineering. He has coauthored more than 110 articles in international journals and 160 at international conferences. He has made scientific contributions to higher symmetries, transformation optics, lens antennas, metasurfaces, leaky wave antennas and high-impedance surfaces.

Dr. Quevedo-Teruel was the EurAAP delegate for Sweden, Norway, and Iceland, from 2018 to 2020, and he has been a member of the EurAAP Board of Directors since January 2021. Since January 2022, he has been the Vice-Chair of EurAAP. He has been the Chair of the IEEE APS Educational Initiatives Program since 2020. He was a Distinguished Lecturer of the IEEE Antennas and Propagation Society for the period of 2019–2021. He has been an Associate Editor of the IEEE TRANSACTIONS ON ANTENNAS AND PROPAGATION since 2018 and is the Founder and the Editor-in-Chief of the EurAAP Journal *Reviews of Electromagnetics* since 2020.